

## Neutron capture cross section measurements of <sup>241</sup>Am at the n\_TOF facility

A. Oprea<sup>1,\*</sup>, F. Gunsing<sup>2</sup>, P. Schillebeeckx<sup>3</sup>, O. Aberle<sup>4</sup>, M. Bacak<sup>4,5,2</sup>, E. Berthoumieux<sup>2</sup>, D. Cano-Ott<sup>6</sup>, M. Diakaki<sup>7,4</sup>, E. Dupont<sup>2</sup>, B. Geslot<sup>8</sup>, T. Glodariu<sup>†1</sup>, J. Heyse<sup>3</sup>, E. Mendoza<sup>6</sup>, A. Negret<sup>1</sup>, V. Alcayne<sup>6</sup>, S. Amaducci<sup>9,10</sup>, J. Andrzejewski<sup>11</sup>, L. Audouin<sup>12</sup>, V. Bécaries<sup>6</sup>, V. Babiano-Suarez<sup>13</sup>, M. Barbagallo<sup>4,14</sup>, F. Bečvář<sup>15</sup>, G. Bellia<sup>9,10</sup>, J. Billowes<sup>16</sup>, D. Bosnar<sup>17</sup>, A. Brown<sup>18</sup>, M. Busso<sup>14,19,20</sup>, M. Caamaño<sup>21</sup>, L. Caballero-Ontanaya<sup>13</sup>, F. Calviño<sup>22</sup>, M. Calviani<sup>4</sup>, A. Casanovas<sup>22</sup>, F. Cerutti<sup>4</sup>, Y. H. Chen<sup>12</sup>, E. Chiaveri<sup>4,16,23</sup>, N. Colonna<sup>14</sup>, G. Cortés<sup>22</sup>, M. A. Cortés-Giraldo<sup>23</sup>, L. Cosentino<sup>9</sup>, S. Cristallo<sup>14,19,24</sup>, L. A. Damone<sup>14,25</sup>, M. Dietz<sup>26</sup>, C. Domingo-Pardo<sup>13</sup>, R. Dressler<sup>27</sup>, I. Durán<sup>21</sup>, Z. Eleme<sup>28</sup>, B. Fernández-Domínguez<sup>21</sup>, A. Ferrari<sup>4</sup>, P. Finocchiaro<sup>9</sup>, V. Furman<sup>29</sup>, K. Göbel<sup>30</sup>, R. Garg<sup>26</sup>, A. Gawlik<sup>11</sup>, S. Gilardoni<sup>4</sup>, I. F. Gonçalves<sup>31</sup>, E. González-Romero<sup>6</sup>, C. Guerrero<sup>23</sup>, H. Harada<sup>32</sup>, S. Heinitz<sup>27</sup>, D. G. Jenkins<sup>18</sup>, E. Jericha<sup>5</sup>, F. Käppeler<sup>33</sup>, Y. Kadi<sup>4</sup>, A. Kimura<sup>32</sup>, N. Kivel<sup>27</sup>, M. Kokkoris<sup>7</sup>, Y. Kopatch<sup>29</sup>, M. Krtička<sup>15</sup>, D. Kurtulgil<sup>30</sup>, I. Ladarescu<sup>13</sup>, C. Lederer-Woods<sup>26</sup>, J. Leredegui-Marco<sup>23</sup>, S. Lo Meo<sup>34,35</sup>, S. J. Lonsdale<sup>26</sup>, D. Macina<sup>4</sup>, A. Manna<sup>35,36</sup>, T. Martínez<sup>6</sup>, A. Masi<sup>4</sup>, C. Massimi<sup>35,36</sup>, P. Mastinu<sup>37</sup>, M. Mastromarco<sup>4</sup>, F. Matteucci<sup>38,39</sup>, E. A. Mauger<sup>27</sup>, A. Mazzone<sup>14,40</sup>, A. Mengoni<sup>34</sup>, V. Michalopoulou<sup>7</sup>, P. M. Milazzo<sup>38</sup>, F. Mingrone<sup>4</sup>, A. Musumarra<sup>9,41</sup>, R. Nolte<sup>42</sup>, F. Ogállar<sup>43</sup>, N. Patronis<sup>28</sup>, A. Pavlik<sup>44</sup>, J. Perkowski<sup>11</sup>, L. Persanti<sup>14,19,24</sup>, I. Porras<sup>43</sup>, J. Praena<sup>43</sup>, J. M. Quesada<sup>23</sup>, D. Radeck<sup>42</sup>, D. Ramos-Doval<sup>12</sup>, R. Reifarh<sup>30</sup>, D. Rochman<sup>27</sup>, C. Rubbia<sup>4</sup>, M. Sabaté-Gilarte<sup>4,23</sup>, A. Saxena<sup>45</sup>, D. Schumann<sup>27</sup>, A. G. Smith<sup>16</sup>, N. V. Sosnin<sup>16</sup>, A. Stamatopoulos<sup>7</sup>, G. Tagliente<sup>14</sup>, J. L. Tain<sup>13</sup>, T. Talip<sup>27</sup>, A. Tarifeño-Saldivia<sup>22</sup>, L. Tassan-Got<sup>4,7,12</sup>, P. Torres-Sánchez<sup>43</sup>, A. Tsinganis<sup>4</sup>, J. Ulrich<sup>27</sup>, S. Urlass<sup>4,46</sup>, S. Valenta<sup>15</sup>, G. Vannini<sup>35,36</sup>, V. Variale<sup>14</sup>, P. Vaz<sup>31</sup>, A. Ventura<sup>35</sup>, V. Vlachoudis<sup>4</sup>, R. Vlastou<sup>7</sup>, A. Wallner<sup>47</sup>, P. J. Woods<sup>26</sup>, T. Wright<sup>16</sup>, and P. Žugec<sup>17</sup> (The n\_TOF Collaboration)

<sup>1</sup>Horia Hulubei National Institute of Physics and Nuclear Engineering, Romania

<sup>2</sup>CEA Ifru, Université Paris-Saclay, F-91191 Gif-sur-Yvette, France

<sup>3</sup>European Commission, Joint Research Centre, Geel, Retieseweg 111, B-2440 Geel, Belgium

<sup>4</sup>European Organization for Nuclear Research (CERN), Switzerland

<sup>5</sup>Technische Universität Wien, Austria

<sup>6</sup>Centro de Investigaciones Energéticas Medioambientales y Tecnológicas (CIEMAT), Spain

<sup>7</sup>National Technical University of Athens, Greece

<sup>8</sup>DEN/CAD/DER/SPEX/LPE, CEA Cadarache, Saint-Paul-les-Durance 13108, France

<sup>9</sup>INFN Laboratori Nazionali del Sud, Catania, Italy

<sup>10</sup>Dipartimento di Fisica e Astronomia, Università di Catania, Italy

<sup>11</sup>University of Lodz, Poland

<sup>12</sup>Institut de Physique Nucléaire, CNRS-IN2P3, Univ. Paris-Sud, Université Paris-Saclay, F-91406 Orsay Cedex, France

<sup>13</sup>Instituto de Física Corpuscular, CSIC - Universidad de Valencia, Spain

<sup>14</sup>Istituto Nazionale di Fisica Nucleare, Sezione di Bari, Italy

<sup>15</sup>Charles University, Prague, Czech Republic

<sup>16</sup>University of Manchester, United Kingdom

<sup>17</sup>Department of Physics, Faculty of Science, University of Zagreb, Zagreb, Croatia

<sup>18</sup>University of York, United Kingdom

<sup>19</sup>Istituto Nazionale di Fisica Nucleare, Sezione di Perugia, Italy

<sup>20</sup>Dipartimento di Fisica e Geologia, Università di Perugia, Italy

<sup>21</sup>University of Santiago de Compostela, Spain

<sup>22</sup>Universitat Politècnica de Catalunya, Spain

<sup>23</sup>Universidad de Sevilla, Spain

<sup>24</sup>Istituto Nazionale di Astrofisica - Osservatorio Astronomico di Teramo, Italy

<sup>25</sup>Dipartimento di Fisica, Università degli Studi di Bari, Italy

<sup>26</sup>School of Physics and Astronomy, University of Edinburgh, United Kingdom

<sup>27</sup>Paul Scherrer Institut (PSI), Villigen, Switzerland

<sup>28</sup>University of Ioannina, Greece

<sup>29</sup>Joint Institute for Nuclear Research (JINR), Dubna, Russia

<sup>30</sup>Goethe University Frankfurt, Germany

<sup>31</sup>Instituto Superior Técnico, Lisbon, Portugal

<sup>32</sup>Japan Atomic Energy Agency (JAEA), Tokai-mura, Japan

<sup>33</sup>Karlsruhe Institute of Technology, Campus North, IKP, 76021 Karlsruhe, Germany

<sup>34</sup>Agenzia nazionale per le nuove tecnologie (ENEA), Bologna, Italy

<sup>35</sup>Istituto Nazionale di Fisica Nucleare, Sezione di Bologna, Italy

<sup>36</sup>Dipartimento di Fisica e Astronomia, Università di Bologna, Italy

<sup>37</sup>Istituto Nazionale di Fisica Nucleare, Sezione di Legnaro, Italy

<sup>38</sup>Istituto Nazionale di Fisica Nucleare, Sezione di Trieste, Italy

<sup>39</sup>Dipartimento di Astronomia, Università di Trieste, Italy

<sup>40</sup>Consiglio Nazionale delle Ricerche, Bari, Italy

<sup>41</sup>Dipartimento di Fisica e Astronomia, Università di Catania, Italy

<sup>42</sup>Physikalisch-Technische Bundesanstalt (PTB), Bundesallee 100, 38116 Braunschweig, Germany

<sup>43</sup>University of Granada, Spain

<sup>44</sup>University of Vienna, Faculty of Physics, Vienna, Austria

<sup>45</sup>Bhabha Atomic Research Centre (BARC), India

<sup>46</sup>Helmholtz-Zentrum Dresden-Rossendorf, Germany

<sup>47</sup>Australian National University, Canberra, Australia

**Abstract.** Neutron capture on  $^{241}\text{Am}$  plays an important role in the nuclear energy production and also provides valuable information for the improvement of nuclear models and the statistical interpretation of the nuclear properties. A new experiment to measure the  $^{241}\text{Am}(n,\gamma)$  cross section in the thermal region and the first few resonances below 10 eV has been carried out at EAR2 of the n\_TOF facility at CERN. Three neutron-insensitive  $\text{C}_6\text{D}_6$  detectors have been used to measure the neutron-capture gamma cascade as a function of the neutron time of flight, and then deduce the neutron capture yield. Preliminary results will be presented and compared with previously obtained results at the same facility in EAR1. In EAR1 the gamma-ray background at thermal energies was about 90% of the signal while in EAR2 is up to a 25 factor much more favorable signal to noise ratio. We also extended the low energy limit down to subthermal energies. This measurement will allow a comparison with neutron capture measurements conducted at reactors and using a different experimental technique.

## 1 Introduction and motivation

The design and modelling of advanced nuclear systems and nuclear fuel cycles need detailed knowledge of the nuclear data of the most relevant isotopes, including nuclear reaction cross sections and decay data. In particular, accurate knowledge of the neutron capture cross section of  $^{241}\text{Am}(n,\gamma)$  is required since it plays an important role in the nuclear energy production and fuel cycle scenarios. For this reason, the isotope  $^{241}\text{Am}$  is listed in the NEA High Priority Request List [1, 2]. Cross section data can also provide valuable nuclear structure data necessary for the improvement of nuclear models and the statistical interpretation of the nuclear properties.

The neutron capture cross section of  $^{241}\text{Am}$  is an important quantity for nuclear technology applications. The nuclei  $^{241}\text{Am}$  and  $^{237}\text{Np}$  are the minor actinides which contribute most to the long-term hazard of nuclear waste, as  $^{241}\text{Am}$  (half life  $T_{1/2} = 432$  y) decays via  $\alpha$  decay into  $^{237}\text{Np}$  ( $T_{1/2} = 2$  My). After Np, Am is the second most abundant minor actinide present in spent nuclear fuel, of which  $^{241}\text{Am}$  is the most abundant isotope. The build-up of heavier actinides like Cm, goes through  $(n,\gamma)$  reactions on Am isotopes. The  $^{241}\text{Am}(n,\gamma)$  reaction leads to  $^{242}\text{Cm}$  production via the decay of the nucleus  $^{242}\text{Am}$  ( $T_{1/2} = 16$  h).  $^{242}\text{Cm}$  decays via  $\alpha$  emission into  $^{238}\text{Pu}$ , which is fissile in a fast spectrum.

The discrepancies observed between experimental and evaluated data sets in the  $^{241}\text{Am}$  neutron capture cross section has triggered an interest for new measurements. Several time-of-flight measurements of  $^{241}\text{Am}(n,\gamma)$  reaction have been performed in the last years: Jandel *et al.* [3] in Los Alamos National Laboratory, using the  $4\pi$  calorimeter of  $\text{BaF}_2$  crystals DANCE. Lampoudis *et al.* [4] at the

GELINA facility in Geel, Belgium used two liquid scintillator detectors based on deuterated benzene ( $\text{C}_6\text{D}_6$ ). At the n\_TOF facility at CERN, two measurements have been performed in the past, both at the 185 m flight path of EAR1. One measurement was done with  $\text{C}_6\text{D}_6$  detectors by Fraval *et al.* [5], and the other using the  $\text{BaF}_2$  total absorption calorimeter (TAC) by Mendoza *et al.* [6]. Both experiments were using the same  $^{241}\text{Am}$  sample. The results of the two EAR1 measurements present sizeable differences at low energy below 10 eV, but were still in agreement within the quoted uncertainties. Both measurements suffer from a large systematic uncertainty at low neutron energy caused by the large background component due to the radioactivity of  $^{241}\text{Am}$ . Indeed for these measurements in EAR1 the gamma-ray background at thermal energies was about 90% of the signal.

In order to improve the accuracy on the neutron induced cross sections of  $^{241}\text{Am}$  in the low energy region, a new neutron capture measurement has been performed at the neutron time-of-flight facility n\_TOF at CERN. This time the measurement was done at the new flight path EAR2 [7], located 20 m vertically from the neutron spallation source. Due to the much higher neutron flux, EAR2 is more suited for highly radioactive isotopes. The focus of this measurement is on the resolved energy region and in particular the thermal region and the first resonances below 10 eV. A comparison with previous reported results is further presented.

## 2 Experimental setup

### 2.1 The n\_TOF facility

The n\_TOF facility is located at CERN (European Organization for Nuclear Research) and has been described else-

\*e-mail: andreea.oprea@nipne.ro

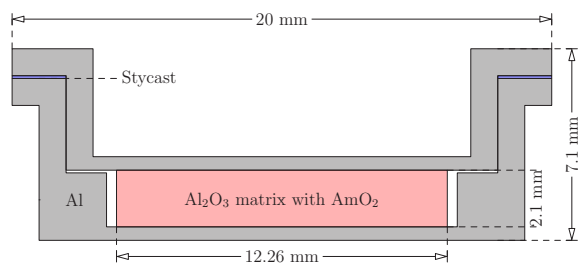


**Figure 1.** A schematic view of the  $^{241}\text{Am}$  sample used in the experiment.

where [8]. The neutron beam is generated through spallation of 20 GeV/c protons extracted in pulses from the Proton Synchrotron (PS) and impinging on a 40 cm thick and 60 cm diameter cylindrical lead target. The proton pulses are delivered with a time spread of 7 ns (rms), having a nominal intensity of  $7 \times 10^{12}$  protons per pulse at a minimum repetition rate of 1.2 s, leading into a very high instantaneous neutron flux. After moderation of the initially fast neutrons, a wide-spectrum neutron beam is produced from thermal to a few GeV. Two experimental areas where experiments are mounted are available at the n\_TOF facility: EAR1 [9], having a horizontal flight path of about 185 m from the spallation lead target, and EAR2 [7], with a vertical flight path of about 20 m.

Since the beam line of the vertical beam is about 10 times shorter, the available neutron flux per proton pulse in EAR2 is considerably higher than in EAR1 [10]. Therefore EAR2 is particularly suited for measuring highly radioactive samples. In addition, due to the approximately 10 times shorter flight distance, the time-of-flight interval needed to cover a range of neutron energies, is 10 times smaller. This results in an additional increase of a factor 10 of the signal to noise ratio due to radioactivity. On the other hand, the excellent energy resolution at EAR1, due to the large flight distance, cannot be reached at EAR2.

## 2.2 Data acquisition

The Data Acquisition System (DAQ) has been upgraded to 175 MSample digitizers from Teledyne SP Devices with a sampling frequency of up to 2 GHz and an amplitude resolution of 12 or 14 bit. The acquired waveforms are, after zero-suppression, automatically transferred from the DAQ computers to the CERN Advanced STORage manager (CASTOR) for long-term storage and off-line analysis. The larger on-board memory has increased the exploitable time-of-flight range with respect to the previous DAQ system, and is now expanded down to thermal neutron energies for both EAR1 and EAR2. The DAQ is triggered by each proton pulse and records detector signals during a time window of 100 ms.

## 2.3 The $^{241}\text{Am}$ sample

Two  $^{241}\text{Am}$  samples were used for this experiment. Each sample consists of americium oxide ( $^{241}\text{AmO}_2$ ), infiltrated

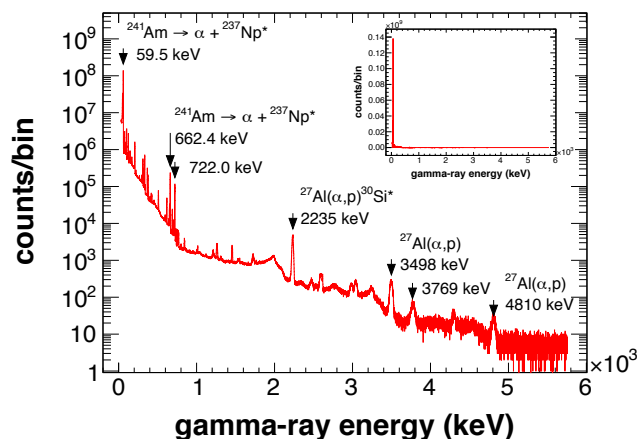


**Figure 2.** The  $\gamma$ -ray spectrum of the  $^{241}\text{Am}$  sample measured with HPGe setup BANEX of the actinide facility in CEA Cadarache. Several characteristic  $\gamma$  rays from  $\alpha$ -induced reactions are shown as well. The  $^{241}\text{Am}$  sample activity in linear scale is shown in the inset illustrating the very strong 59.5 keV line dominating the activity spectrum.

and immobilized in an aluminum oxide ( $\text{Al}_2\text{O}_3$ ) pressed pellet forming a rigid disk of 12.26 mm diameter. The disk was then encapsulated in an aluminum container and sealed with Stycast as illustrated in figure 1.

The first sample, labelled IRMM1, has a mass of  $32.23 \pm 0.19$ -mg and was the same sample as used in the previous n\_TOF capture experiments [5, 6]. A second sample, labelled IRMM4, has a  $40.98 \pm 0.25$  mg content of  $^{241}\text{Am}$ . The masses were determined by calorimetry [11]. The radioactivity of the IRMM1 sample was about 4.1 GBq while for the IRMM4 was about 5.1 GBq. More details on the  $^{241}\text{Am}$  sample composition are presented in table 1.

Several nearly identical dummy (or blank) samples, without americium oxide inside the  $\text{Al}_2\text{O}_3$  disk, and also encapsulated inside an aluminium canning, were also produced. The one that was used in the previous measurements at n\_TOF appeared to contain a broken  $\text{Al}_2\text{O}_3$  pellet which seemed to be assembled with a samarium-containing glue during the production process. This became visible in the neutron capture spectra from that measurement [5] and was later confirmed by an X-ray analysis of the dummy samples. Therefore, for the present measurement we have used one of the other dummy samples, without a noticeable samarium content, for the background measurements.

The  $\alpha$ -activity of the  $^{241}\text{Am}$  sample generated several  $\gamma$ -rays which could be identified as shown in figure 2. In an independent measurement with HPGe setup BANEX of the actinide facility in CEA Cadarache, the full gamma-ray

**Table 1.** The material quantities of the two used  $^{241}\text{Am}$  samples.

sample ID	$^{241}\text{Am}$ (mg)	$\text{Al}_2\text{O}_3$ (mg)
IRMM1	$32.23 \pm 0.19$	305
IRMM4	$40.98 \pm 0.25$	388

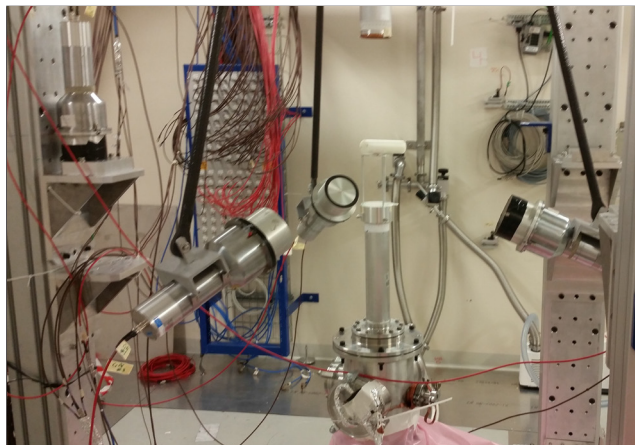


**Figure 3.** The three  $C_6D_6$  scintillation detectors used to measure the capture  $\gamma$ -rays in n\_TOF-EAR2. The additional fourth monitoring detector is also visible on the picture.

spectrum from 40 keV up to 5 MeV was measured. The  $\gamma$ -rays by  $\alpha$ -induced reactions are clearly visible. On the linear scale of the inset of figure 2 it can be seen that the main component of the activity of the  $^{241}Am$  sample is concentrated at the 59.5 keV  $\gamma$ -ray, coming from  $^{237}Np$  following the  $\alpha$ -decay of  $^{241}Am$ .

## 2.4 The $C_6D_6$ detectors

Three  $C_6D_6$  liquid scintillator detectors were used for the  $\gamma$ -ray detection. The main characteristics of these detectors are a very good time resolution and a low sensitivity to scattered neutrons. The very high activity of the  $^{241}Am$  samples draws a large current over the voltage divider of the photomultiplier. To avoid an undesirable detector response due to a strong flux of 59.5 keV  $\gamma$ -rays, a Pb shielding between sample and detector was used in the previous n\_TOF measurements. For the present measurement we have chosen to increase the distance between sample and detector, avoiding the need for a Pb shielding and allowing the possibility to use a lower gamma-ray threshold.

The three detectors and the sample were mounted as shown on the picture in figure 3, together with a schematic view as in figure 4. The sample (shown in red) was placed on a horizontal sample holder, which was fixed with three vertical thin rods of 15 cm long (two are shown on the picture) to the end flange of the evacuated beam pipe. In this way the material directly around the sample was minimized. The detectors were held in place using carbon fibre rods (not shown). The distance between the front face of the scintillator cells and the center of the sample was approximately 40 cm. This distance was chosen to optimize the detector performance in presence of the large radioactivity and the deliberate absence of shielding between the detector and the sample. A fourth  $C_6D_6$  detector was placed even further away from the sample and was only used for monitoring purposes.

Each  $C_6D_6$  detector was energy calibrated using standard  $\gamma$ -ray sources ( $^{137}Cs$ ,  $^{88}Y$ ,  $^{60}Co$  and a mixed Am-Be source).

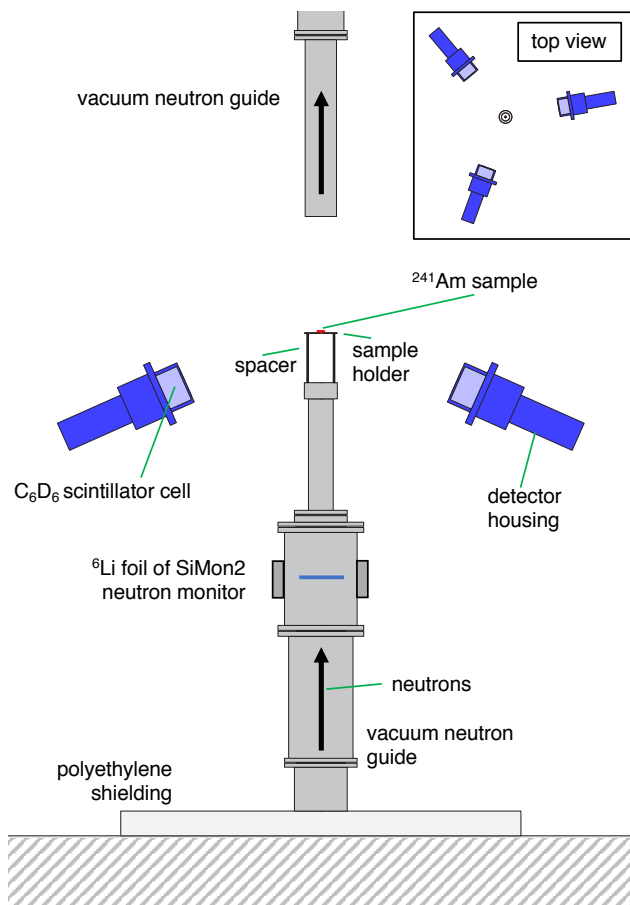


**Figure 4.** A schematic view of the detectors and sample setup used for the present experiment. While the distances in the figure are on scale, for clarity the detectors are not presented in perspective. The distance between detectors and sample is about 50 cm. The inset shows a top view of the set-up with the three-detector configuration.

Supplementary measurements with other samples (dummy sample: Al canning plus the  $Al_2O_3$  matrix, only Al canning, natural C and Pb) were carried out to determine the background. Measurements without beam and without sample (no sample, beam off), with beam but with the sample in place ( $^{241}Am$ , beam off), and with neutron beam but without any sample were also performed. For the absolute normalisation the low-energy saturated resonances of five different samples ( $^{197}Au$ ,  $^{nat}Ag$ ,  $^{103}Rh$ ,  $^{nat}Ir$  and  $^{nat}U$ ) were measured.

## 3 Preliminary results

The main objective of the present work is a precise measurement of the  $^{241}Am(n,\gamma)$  reaction cross section in the thermal energy region and for the first few resonances below 10 eV. In the region below 10 eV the uncertainties of the two previous n\_TOF experiments were very large. This region is particularly important for nuclear fission technology. Experimental data either cover only thermal energies, or are time-of-flight data, but do not include the full thermal region. With the present measurement we com-

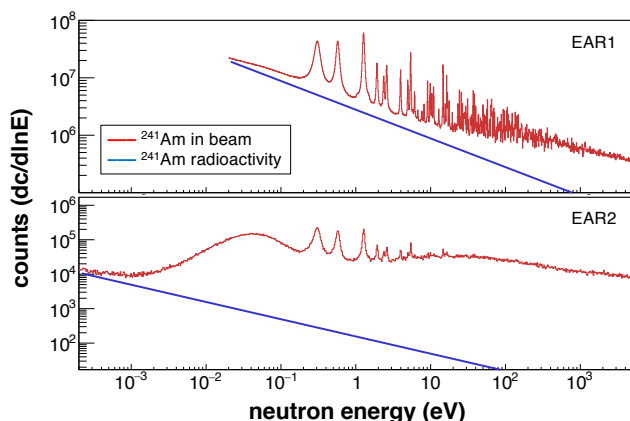


**Figure 5.** Comparison of the  $^{241}\text{Am}$  spectra together with the  $^{241}\text{Am}$  count rate from radioactivity at EAR1 (2010) and EAR2 (2017). The fitted spectrum due to the constant radioactivity, is represented by the blue  $1/\sqrt{E}$  line.

prise both the full thermal region and the resonance region. In addition, the background due to high radioactivity of  $^{241}\text{Am}$  is drastically reduced in n\_TOF-EAR2.

In figure 5 we show the counting spectrum of the  $^{241}\text{Am}(n,\gamma)$  for the present EAR2 experiment. For comparison, also the previous EAR1  $\text{C}_6\text{D}_6$  results [5] are shown on the same neutron energy scale. In order to compare the present results to the previous n\_TOF experiments, in addition to using the same sample (IRMM1), also the same energy threshold of 300 keV was applied to each  $\text{C}_6\text{D}_6$  detector. Still an important difference is the use of a 2 mm Pb shielding for the EAR1 setup, and no shielding in the EAR2 setup. We clearly see the complete thermal peak from the neutron flux present in the EAR2 counting spectrum. In the EAR1 experiment, while the data acquisition system could not record down to this low energy, the thermal neutrons are strongly suppressed by the borated water moderator. The  $^{241}\text{Am}$  spectra from EAR1 presents a visible better energy resolution as compared to EAR2.

In the figure we also see the fit of the radioactivity background. The number of counts per time unit is constant for this spectrum, and shows as a  $1/\sqrt{E}$  in the units used here. Also, compared to the previous measurements performed in EAR1, there is a substantial increase in the

ratio between the capture signal and the radioactivity background of more than a factor 200 in EAR2 due to the increased neutron flux. This is one of the most important features of the n\_TOF facility and essential for the measurement of neutron-induced cross section of highly radioactive targets. Nevertheless, even if the resolution is much less favourable in EAR2, the peak-to-valley ratio of the first strong resonance and the region between the first and second strong resonances, is significantly better for the EAR1 experiment, indicating that the time-dependent background is much better in EAR1. The strong thermal component of the neutron flux in EAR2, which is efficiently suppressed in EAR1, results in a high flux of in-beam 2.2 MeV gamma rays from neutron capture on hydrogen of the water moderator near the spallation target. Those gamma-rays contribute significantly to the time-dependent background in EAR2.

## 4 Conclusion

The here presented counting spectrum shows the capability of n\_TOF EAR2 to perform neutron capture measurements in the low energy range, covering both the full thermal region and the first resonances. The excellent ratio of signals due to neutron capture and due to the radioactivity background is particularly beneficial for a nucleus like  $^{241}\text{Am}$ . At present all data are verified for integrity and consistency and a full analysis of the data is ongoing.

## References

- [1] <https://www.oecd-nea.org/dbdata/hprl/>
- [2] E. Dupont et al. (2019), *these proceedings*
- [3] M. Jandel et al., Phys. Rev. C **78** (2008)
- [4] C. Lampoudis et al., Eur. Phys. J. Plus **128** (2013)
- [5] K. Fraval et al., Phys. Rev. C **89** (2014)
- [6] E. Mendoza et al., Phys. Rev. C **97** (2018)
- [7] C. Weiß et al., Nucl. Instr. Meth. A **799**, 90 (2015)
- [8] E. Chiaveri et al. (2019), *these proceedings*
- [9] C. Guerrero et al., Eur. Phys. J. A **49** (2013)
- [10] M. Sabaté-Gilarte et al., Eur. Phys. J. A **53** (2017)
- [11] H. Tagziria et al., Nucl. Instr. Meth. A **691**, 90 (2012)